# Towards robust sensor fusion for state estimation in airborne applications using GNSS and IMU ⋆

**Fabian Girrbach** [*,**] **Jeroen D. Hol** [*] **Giovanni Bellusci** [*]
**Moritz Diehl** [**]

[*] *are with Xsens Technologies B.V.,7521 PR Enschede, the Netherlands (e-mail: author@xsens.com).*
[**] *are with the University of Freiburg, Department of Microsystems Engineering (IMTEK), Georges-Koehler-Allee 102, 79110 Freiburg, Germany (e-mail: author@imtek.uni-freiburg.de)*

**Abstract:** Precise estimation of position, velocity, and orientation is crucial for robust control in airborne applications such as the fast maneuvering power kites for airborne wind energy generators. In this paper we present a sensor fusion approach for the measurements of a global navigation satellite system receiver and an inertial measurement unit, using methods from direct optimal control. The resulting optimization problem is based on the minimization of the weighted squared residuals between model predictions and measurements and solved using a direct collocation discretization strategy. The framework allows the formulation of a batch and filter estimator which include beside the estimation of the navigational states the identification of sensor parameters such as biases of the inertial measurement unit. The results of the algorithms are evaluated against a reference trajectory of a maneuvering single propeller aircraft and achieve root mean squared errors below 1 m in position, 0.4 $\mathrm{ms}^{-1}$ in velocity, and 0.5 deg in orientation for the batch estimator. The contribution in this paper is a first step towards the required robustness of state estimation for airborne applications.

*Keywords:* Optimal estimation, estimation algorithms, inertial navigation, parameter estimation, moving horizon estimation, orientation and position tracking

## 1. INTRODUCTION

Over the last years, the number of airborne applications has drastically increased. The extensive research in the field of *unmanned aerial vehicles* (UAVs) for tasks like transportation of goods (Iwata, 2013) and surveillance (Perez et al., 2013) already impacts daily processes in agriculture, surveillance of public events, fast delivery of goods and military operations. Furthermore *airborne wind energy* (AWE) systems are on the edge of commercialization. AWE overcomes the major difficulties posed by the exponentially growing size and mass of conventional wind turbine generators (Laks et al., 2009). Its paradigm shift proposes to remove the structural elements not directly involved in power generation, which results in tethered flying turbines (see Ahrens et al. (2013) for an overview). For the commercialization of airborne systems a robust and failure tolerant operation is a crucial factor to gain acceptance by the public.

The requirements regarding safety and robustness in airborne applications impose challenges for the estimation and control algorithms in the presence of high system dynamics and sensor outages. Advanced control strategies such as *nonlinear model predictive control* (NMPC) are investigated (Gros et al., 2012) to cope with the dynamics and allow for a stable control. The impact of measurement errors on the estimation of the system state can be reduced by information fusion of various sensors. Several approaches combining different sets of sensors such as *inertial measurement units* (IMUs), *global navigation satellite system* (GNSS) receivers (Grewal et al., 2007), *ultra-wideband* (UWB) sensors (Hol et al., 2009) and cameras (Grabe et al., 2015) have been proposed, using mostly a Kalman filter based estimation algorithm. Further research has shown the potential of an in-run sensor calibration to improve accuracy and robustness (Vandersteen et al., 2013). For a precise identification of sensor parameters their observability has a crucial impact. Naturally, a batch estimator which uses measurements over a large time window offers increased observability and has therefore the potential to outperform filter based estimation algorithms besides the obvious removal of startup effects.

In this paper we propose an optimization based sensor fusion approach for the estimation of position, velocity, and orientation using onboard measurements. The exclusive usage of GNSS and IMU sensors allows this approach to be applied to a wide range of airborne applications including AWE generators. In comparison to Polóni et al. (2015) the magnetometer is not considered in this paper since magnetic distortions can quickly lead to undesired behavior which may decrease the robustness of the estimator. An optimization framework is proposed which

⋆ Support by the EU via ITN-AWESCO (642 682) is gratefully acknowledged.

comprises a system model to encode the continuous-time dynamics of the system and additionally defines sensor models to account for typical measurement errors such as biases. According to the model equations, sensor measurements are predicted which lead to a residual minimization problem. By applying methods from the field of direct optimal control to sensor fusion, we solve the optimization problem efficiently with an interior point solver using a direct collocation strategy which embeds the integration of the system dynamics inside the optimization problem. The proposed estimation framework enables the formulation and implementation of a batch and filter estimator. In an evaluation against an accurate reference trajectory of a maneuvering single propeller aircraft, we compare the performance of both approaches.

This paper is organized as follows. After introducing the relevant models in Section 2, we formulate the optimization problems for batch and filter estimator in Section 3 and describe the discretization of the problem using direct collocation. In Section 4 we will discuss the experimental results, focusing on the comparison between batch and filter solutions.

## 2. MODEL

The sensor fusion problem contains measured and estimated quantities expressed in several coordinate frames, see Fig. 1. The position and velocity measurements are obtained by the GNSS sensor in the *earth-centered, earth-fixed* (ECEF) frame and often expressed in *latitude, longitude, altitude* (LLA). The measurements are transformed to a locally-fixed and non-moving frame $L$ following the *east, north, up* (ENU) convention with its origin located at a reference location. Since the transformation between the global and local frame is constant over time, the measurements are converted to the local frame $L$ in a preprocessing step. The measurements of the IMU are obtained in the sensor coordinate frame $S$ which is moving w.r.t the local frame $L$. The notation $\cdot^L$ or $\cdot^S$ will be used to indicate measured or estimated variables w.r.t. to the local or sensor frame. The quantities subject to the sensor fusion problem are summarized as the state of the system over time $\boldsymbol{x}(t)$. The state of the system is propagated according to the dynamics of the model $\dot{\boldsymbol{x}}(t) = f(\boldsymbol{x}(t), \boldsymbol{u}(t))$ driven by the control input $\boldsymbol{u}(t)$. Further output functions are defined which predict measurements using the states and controls and allow the formulation of squared weighted residuals between measured and estimated quantities.

### *2.1 Dynamics*

A piecewise-constant linear acceleration and angular velocity model is used to model the translational and rotational motion,

$$\dot{p}^L(t) = v^L(t), \tag{1a}$$

$$\dot{v}^L(t) = a^L(t), \tag{1b}$$

$$\dot{q}^{LS}(t) = \tfrac{1}{2} q^{LS}(t) \odot \omega^S_{LS}(t). \tag{1c}$$

The position $p^L(t) \in \mathbb{R}^3$ and velocity $v^L(t) \in \mathbb{R}^3$ are obtained by integration of the acceleration $a^L(t) \in \mathbb{R}^3$. The angular velocity $\omega^S_{LS} \in \mathbb{R}^3$ from the $S$-frame to the $L$-frame expressed in the $S$-frame drives the *ordinary differential equation* (ODE) of the orientation, which is parametrized by a unit quaternion $q^{LS}(t) \in \mathbb{R}^4, \forall t : \|q^{LS}(t)\|_2 = 1$ describing the orientation between the $S$ and $L$-frame. The $\odot$ operator is introduced for the product of a quaternion $q = (q_0, q_v) \in \mathbb{R}^4$ and a vector $r \in \mathbb{R}^3$

$$q \odot r := [-q_v \cdot r, q_0 r + q_v \times r]\,. \tag{2}$$

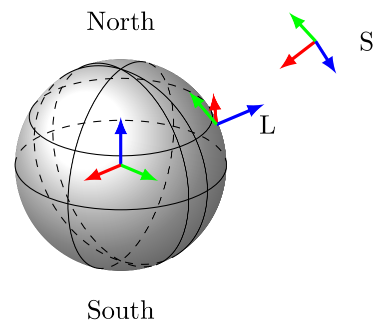


Fig. 1. The various navigation frames. Showing the fixed frames (ECEF and $L$) and the free moving $S$-frame.

### *2.2 Measurements*

The GNSS sensor measures position $p^L$ and velocity $v^L$ with a sampling time $T_{\mathrm{GNSS}}$. We define output functions

$$y^L_p(\boldsymbol{x}, \boldsymbol{u}, t_k) = p^L(t_k), \tag{3a}$$

$$y^L_v(\boldsymbol{x}, \boldsymbol{u}, t_k) = v^L(t_k), \tag{3b}$$

which relate the GNSS measurements directly to the state $\boldsymbol{x}(t)$ and define a concatenated GNSS measurement

$$\boldsymbol{y}^L_{\mathrm{GNSS}}(\boldsymbol{x}, \boldsymbol{u}, t_k) = \left[y^L_p(\boldsymbol{x}, \boldsymbol{u}, t_k)^T, y^L_v(\boldsymbol{x}, \boldsymbol{u}, t_k)^T\right]^T, \tag{4}$$

to predict the measurement based on the state $\boldsymbol{x}(t_k)$ for $t_k = T_{\mathrm{GNSS}} k,\ k = 1, \ldots, N$.

The inertial quantities acceleration $a^S \in \mathbb{R}^3$ and angular velocity $\omega^S_{LS}$ are acquired by the IMU at discrete sampling times $T_{\mathrm{IMU}}$, where $T_{\mathrm{GNSS}} \gg T_{\mathrm{IMU}}$. The higher sampled IMU data is integrated between two consecutive GNSS measurements and expressed as motion increments (Savage, 1998). The increments are converted to an average inertial measurement over the interval $[t_k, t_{k+1}]$ and can be predicted using

$$y^S_a(\boldsymbol{x}, \boldsymbol{u}, t_k) = R(q^{LS}(t_k)^{-1}, a^L(t_k) - g^L) + \delta^S_a(t_k), \tag{5a}$$

$$y^S_\omega(\boldsymbol{x}, \boldsymbol{u}, t_k) = \omega^S_{LS}(t_k) + \delta^S_\omega(t_k), \tag{5b}$$

where $g^L$ stands for the constant gravity vector in the $L$ frame and $R(q, r)$ denotes the rotation of a vector $r$ by an unit quaternion $q$. The *micro-machined electromechanical system* (MEMS) accelerometer and gyroscope are modeled using an additive bias term $\delta^S$ for the compensation of measurement offsets (Titterton and Weston, 2004). These biases $\delta^S_a \in \mathbb{R}^3$ and $\delta^S_\omega \in \mathbb{R}^3$ are modeled as constants

$$\dot{\delta}^S_a(t) = [0, 0, 0]^T, \tag{6a}$$

$$\dot{\delta}^S_\omega(t) = [0, 0, 0]^T. \tag{6b}$$

For notational convenience we define again a concatenated IMU measurement

$$\boldsymbol{y}^S_{\mathrm{IMU}}(\boldsymbol{x}, \boldsymbol{u}, t_k) = \left[y^S_a(\boldsymbol{x}, \boldsymbol{u}, t_k)^T, y^S_\omega(\boldsymbol{x}, \boldsymbol{u}, t_k)^T\right]^T. \tag{7}$$

The system dynamics and the sensor models as described above lead to the definition of the state vector and control vector

$$\boldsymbol{x}(t) = \left[p^L(t)^T, v^L(t)^T, q^{LS}(t)^T, \delta_a^S(t)^T, \delta_\omega^S(t)^T\right]^T \quad (8)$$

$$\boldsymbol{u}(t) = \left[a^L(t)^T, \omega_{LS}^S(t)^T\right]^T \quad (9)$$

with dimensions $\boldsymbol{x}(t) \in \mathbb{R}^{N_x}, N_x = 16$ and $\boldsymbol{u}(t) \in \mathbb{R}^{N_u}, N_u = 6$.

## 3. OPTIMIZATION PROBLEM

In this paper a batch and filter approach is presented enabling optimization based sensor fusion and estimation. We will first define common parts before stating the individual optimization problems.

### 3.1 Measurement residuals

The cost function of the optimal estimation problem is defined by the squared weighted sum of residuals between the estimated output variables $\boldsymbol{y}_k$ and the measurements $\bar{\boldsymbol{y}}_k$ at sampling times $t_k$. The residuals are defined by

$$r_{\text{GNSS}}(\boldsymbol{x}, \boldsymbol{u}) = \boldsymbol{y}_{\text{GNSS}}^L(\boldsymbol{x}, \boldsymbol{u}, t_k) - \bar{\boldsymbol{y}}_{\text{GNSS},k}^L, \quad (10a)$$

$$r_{\text{IMU}}(\boldsymbol{x}, \boldsymbol{u}) = \boldsymbol{y}_{\text{IMU}}^S(\boldsymbol{x}, \boldsymbol{u}, t_k) - \bar{\boldsymbol{y}}_{\text{IMU},k}^S, \quad (10b)$$

and evaluate the continuous output functions (4), (7) for the state $\boldsymbol{x}(t)$ and controls $\boldsymbol{u}(t)$ at time $t_k$. The residuals are weighted using matrices $W_k$ and $Q_k$ which contain the inverse of the measurement noise variances.

### 3.2 Direct collocation

We discretize the continuous functions of states $\boldsymbol{x}(t)$ and controls $\boldsymbol{u}(t)$ using the time grid $t_{0:N}$ defined by the sampling time $T_{\text{GNSS}}$. This leads to the discrete sets of states $\mathcal{X} = \{\boldsymbol{x}_0 \dots \boldsymbol{x}_N\}$ and controls $\mathcal{U} = \{\boldsymbol{u}_0 \dots \boldsymbol{u}_{N-1}\}$. Whereas the the control input $\boldsymbol{u}_k$ is piecewise constant for the interval $[t_k, t_{k+1}]$, we approximate the state trajectory between the discretized states by a collocation polynomial $C_k(t)$ which is defined by the weighted sum of $M$ orthogonal Lagrange polynomials, where $M > 1$ defines the degree of the resulting polynomial approximation for each variable in $\boldsymbol{x}$.

$$\begin{aligned} \boldsymbol{x}(t_k + T) &\approx C(\boldsymbol{x}_k, \boldsymbol{c}_k, \tau) \quad (11) \\ &= \sum\nolimits_{m=0}^{M} \sum\nolimits_{n=0}^{N_x} c_{k,mn} e_n P_m(\tau), \quad \boldsymbol{c}_{k,0} = \boldsymbol{x}_k \end{aligned}$$

The collocation points $\tau_{1:M} \in [0, 1]$ are chosen according to the Radau scheme as in Kameswaran and Biegler (2008) for which $\tau_M = 1$. The numerical integration enters the optimization problem over the collocation states $\mathcal{C} = \{\boldsymbol{c}_0 \dots \boldsymbol{c}_{N-1}\}$, where $\boldsymbol{c}_{0:N-1} \in \mathbb{R}^{N_x \times M}$.

The discretization of state trajectory $\boldsymbol{x}_{0:N}$ and the numerical integration using collocation variables $\boldsymbol{c}_{0:N-1}$ increases the number of optimization variables or so called decision variables. To retrieve a physically meaningful trajectory of the state, the collocation variables need to be constrained. To enforce that the polynomial $C_k$ corresponds to the integration of the system dynamics, we constrain the derivative of the scaled polynomials at the collocation points $\tau_{1:M}$ to the ODE of the system $f(\boldsymbol{x}(t), \boldsymbol{u}(t))$ evaluated at the same point using equality constraints. We obtain $M$ equality constraints for each time interval $[t_k, t_{k+1}]$ defined by

$$\frac{\partial}{\partial \tau} C_k(\boldsymbol{x}_k, \boldsymbol{c}_k, \tau)|_{\tau_m} T_{\text{GNSS}}^{-1} = f(\boldsymbol{x}(t_k + \tau_m T_{\text{GNSS}}), \boldsymbol{u}_k), \quad m = 1 \dots M, k = 0 \dots N. \quad (12)$$

An additional continuity constraints defined by

$$\boldsymbol{x}_{k+1} = C(\boldsymbol{x}_k, \boldsymbol{c}_k, \tau_M), \quad k = 0, \dots, N-1, \quad (13)$$

is required to obtain a closed state trajectory after the discretization.

### 3.3 Batch problem

Considering all available measurements over a large time horizon $[t_0, t_N]$ for finding a optimal solution to the sensor fusion problem is considered a batch approach. After defining the set of decision variables and constraints induced by the direct collocation approach, we can state the batch estimation problem over a estimation horizon $N$ as one optimization problem defined by

$$\begin{aligned} \underset{\mathcal{X}, \mathcal{C}, \mathcal{U}}{\text{minimize}} \quad & \frac{1}{2} \sum\nolimits_{k=0}^{N} \|r_{\text{GNSS}}(\boldsymbol{x}_k, \boldsymbol{u}_k)\|_{W_k}^2 \quad (14a) \\ & + \frac{1}{2} \sum\nolimits_{k=0}^{N-1} \|r_{\text{IMU}}(\boldsymbol{x}_k, \boldsymbol{u}_k)\|_{Q_k}^2 \\ \text{subject to} \quad & \\ & Z_q \boldsymbol{x}_0 (Z_q \boldsymbol{x}_0)^T = 1, \quad (14b) \\ & \boldsymbol{x}_{k+1} = C(\boldsymbol{x}_k, \boldsymbol{c}_k, \tau), \quad k = 0, \dots, N-1, \quad (14c) \\ & g_j(\boldsymbol{x}_k, \boldsymbol{c}_k, \tau_{1:M}) = 0, \quad j = 1, \dots, M, \quad k = 0, \dots, N-1 \quad (14d) \end{aligned}$$

Since the quaternion is an over-parametrization of a rotation, we have to guarantee that the estimated quaternions satisfy the unit norm condition. The ODE of a quaternion (1c) preserves the unit norm, which allows to add a single unit norm constraint for the estimation horizon (14b). The constraint is expressed using the selection matrix $Z_q \in \mathbb{R}^{4 \times N_x}$ for the quaternion entries of the state vector $\boldsymbol{x}_k$. The collocation constraint (14d) represents a shorthand formulation for the equality defined in (12).

### 3.4 Initialization

Crucial for every kind of nonlinear optimization is the initialization of the decision variables. To initialize the state $\mathcal{X}$ and control vectors $\mathcal{U}$, we first compute the initial orientation $q_0^{LS}$ using the velocity vector of the first GNSS measurement $\bar{y}_{v,0}^L$ assuming the system obeys nonholonomic constraints and has sufficient speed. The gyroscope measurements of the IMU are used to dead-reckon the orientation trajectory $q_{1:N}^{LS}$, which can be further used to initialize $a_{0:N-1}^L$ using the accelerometer measurements. The biases $\delta_{a,0:N}^S$ and $\delta_{\omega,0:N}^S$ are assumed to be small and therefore initialized to 0. Finally the available sensor measurements $\bar{y}_{p,0:N}^L$, $\bar{y}_{v,0:N}^L$ and $\bar{y}_{\omega,0:N}^S$ are used to assign the not yet initialized variables in state and control vectors. After the full initialization of the state trajectory $\boldsymbol{x}_{0:N}$, we interpolate linearly to initialize the collocation states $\boldsymbol{c}_k$ for $k = 0, \dots, N$ in between two sequential states $[\boldsymbol{x}_k, \boldsymbol{x}_{k+1}]$.

### 3.5 Filter problem

Instead of optimizing using the whole set of measurements, we add recursively measurements to the problem while keeping the window length at $N = 1$. The past information is taken into account using an additional arrival cost term

$$\frac{1}{2}\|\boldsymbol{x}_k - \boldsymbol{x}_{k,0}\|^2_{\Sigma^{-1}_{k,0}} \tag{15}$$

where $\boldsymbol{x}_k$ is the current state and $\boldsymbol{x}_{k,0}$ the prediction of state $\boldsymbol{x}_k$ before optimizing. In other words, (15) penalizes during the optimization deviations from the initial prediction $\boldsymbol{x}_{k,0}$ which is constant for each single optimization problem. The arrival cost is weighted by the inverse of the covariance $\Sigma^{-1}_{k,0}$, which is the predicted covariance of the state $\boldsymbol{x}_k$ calculated in the previous filter iteration. This way, the predicted mean and covariance of $\boldsymbol{x}_{k+1}$ are used in the arrival cost of the next filter iteration which compares to the prediction step in traditional Kalman filtering.

$$\underset{\substack{\boldsymbol{x}_k,\boldsymbol{c}_k,\boldsymbol{u}_k,\\ \boldsymbol{x}_{k+1}}}{\text{minimize}} \quad \frac{1}{2}\|r_{\text{GNSS}}(\boldsymbol{x}_k,\boldsymbol{u}_k)\|^2_{W_k} \tag{16a}$$

$$+\frac{1}{2}\|r_{\text{IMU}}(\boldsymbol{x}_k,\boldsymbol{u}_k)\|^2_{Q_k}+$$

subject to

$$Z_q\boldsymbol{x}_k(Z_q\boldsymbol{x}_k)^T = 1, \tag{16b}$$

$$\boldsymbol{x}_{k+1} = C(\boldsymbol{x}_k, \boldsymbol{c}_k, \tau), \tag{16c}$$

$$g_j(\boldsymbol{x}_k, \boldsymbol{c}_k, \tau_{1:M}) = 0, \qquad j = 1, \dots, M \tag{16d}$$

For the filter it is required to initialize the covariance of the state $\hat{\Sigma}_{0,0}$. Under the assumption that initialization errors are independent, we can initialize using a diagonal matrix of reasonable standard deviations for the initial state $\boldsymbol{x}_0$.

### *3.6 Implementation*

The optimization problem was formulated using the Python interface for the symbolic framework for numeric optimization CasADi (Andersson, 2013) and solved using the interior point solver IPOPT (Wächter and Biegler, 2006). The symbolic framework allows for algorithmic differentiation of the defined equations and the exact Hessian of the Lagrangian is used in the derivative based interior point solver.

## 4. EXPERIMENTAL RESULTS

### *4.1 Measurement setup*

The presented algorithm is evaluated using measurement data from a single propeller aircraft. The data was collected using a Xsens MTi-G-700 [1] tracker which combines an IMU and GNSS sensor in a single package. The device was rigidly attached to a small single propeller aircraft shown in Fig. 2. The sensor frame $S$ was aligned with the body frame which implies that no further transformations were required to retrieve physically meaningful output. The GNSS data $\bar{\boldsymbol{y}}_{\text{GNSS},k}$ was acquired at the maximum rate of 4 Hz and the IMU data $\bar{\boldsymbol{y}}_{\text{IMU},k}$ was streaming motion increments, as described in Section 2, with an output frequency of 4 Hz. In addition, a tactical grade IMU and a differential multi-GNSS sensor were mounted. The tactical grade IMU uses a fiber optic gyroscope with a small drift and solid state accelerometer of high accuracy. For the computation of an accurate trajectory, the GNSS data of the reference sensor was post-processed, time-aligned and fused with the data of the tactical grade IMU in a batch optimization problem (Vydhyanathan et al., 2015). The entire dataset contains several minutes of data, including take-off, different flight maneuvers, and landing. For our analysis we extracted a 360 s long fragment which includes three sharp turns, see Fig. 3.

[1] https://www.xsens.com/products/mti-g-700/


Fig. 2. The Socata single propeller aircraft used for data collection. A Xsens MTi-G-700 tracker and reference sensors (tactical grade IMU, differential GNSS) are rigidly mounted in the space behind the cockpit.

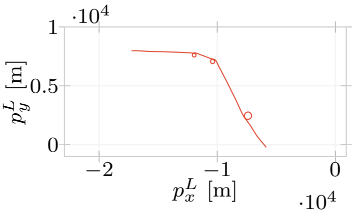


Fig. 3. Trajectory of aircraft used for analysis.

### *4.2 Discussion*

Fig. 4, and 5 show the estimated trajectories of the batch and the filter estimator for velocity $v^L$, and orientation $q^{LS}$. To allow a straight forward interpretation of the orientation, the estimated quaternions $q^{LS}_{0:N}$ are expressed in the Euler angles roll $\phi$, pitch $\theta$ and yaw $\psi$. Due to high velocities, a plot of the positions $p^L$ does not add valuable information for the comparison. Characteristic for fixed-wing flight dynamics we directly observe a correlation between the roll and yaw angles. The *root mean square errors* (RMSEs) for batch and filter estimator in Table 1 reveal smaller errors for the batch estimator. This behavior is expected since initialization errors do not affect directly the final result. For the first 50 s, the aircraft travels on a horizontal flightpath with constant speed. Under these conditions the sensor biases as well as the yaw angle are not observable which results for the filter in non-decreasing standard deviations (see Fig. 8). As the turn is initiated, the variables become observable and the corresponding standard deviation converges.

The estimated orientation results for the yaw angle reveal a four times higher error than for the roll angle and further we notice by inspection of Fig. 5 a small drift in yaw between 100 s and 200 s. During this drift, we observe an expected slowly increasing uncertainty of the yaw estimate in Fig. 8, whereas the other uncertainties converge asymptotically to their final value. The reason for this drift can be well observed in Fig. 6 and Fig. 7 of the accelerometer and gyroscope bias. The biases $\delta_{a,y}$ and $\delta_{\omega,z}$, estimated by the filter, show big offsets compared to

Table 1. RMSEs for batch and filter estimator

| | | Batch | Filter |
|---|---|---|---|
| $p_x^L$ | [m] | 0.7178 | 1.6687 |
| $p_y^L$ | [m] | 0.9931 | 1.6563 |
| $p_z^L$ | [m] | 0.9498 | 0.8261 |
| $v_x^L$ | [ms$^{-1}$] | 0.2254 | 0.3300 |
| $v_y^L$ | [ms$^{-1}$] | 0.3281 | 0.3533 |
| $v_z^L$ | [ms$^{-1}$] | 0.2697 | 0.3012 |
| $\phi$ | [deg] | 0.1279 | 0.5471 |
| $\theta$ | [deg] | 0.4393 | 0.4440 |
| $\psi$ | [deg] | 0.4845 | 2.3014 |

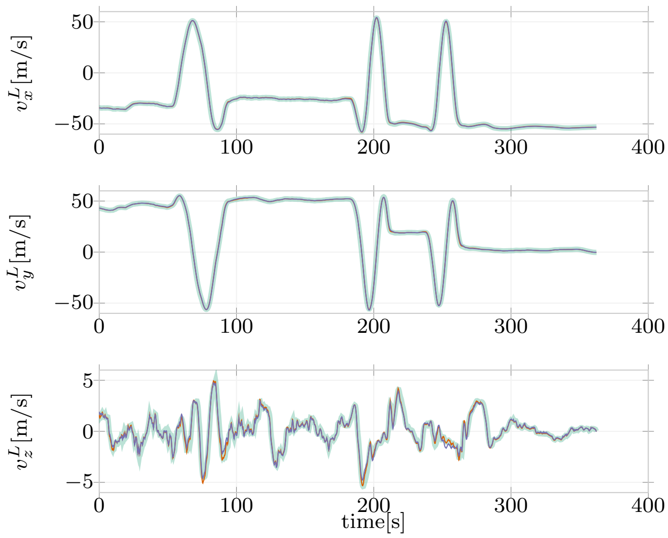


Fig. 4. Estimated batch (—) and filter (—) results for velocity compared reference (—) trajectory.

the batch results. Even though the standard deviations of the biases in Fig. 8 converged after the first turn to their final values further sensor errors and inconsistencies lead to these offsets in the bias estimates and finally to the drift in yaw.

Comparing the plotted standard deviations over time in Fig. 8 for the batch and filter estimator shows lower average standard deviations for the batch estimator than the filter. However in all cases the filter converges to an in magnitude similar standard deviation as for the batch solution, which is a desired behavior for the filter. A comparison between the standard deviations of both estimators and the calculated RMSEs in Table 1 unveils uncertainties several times lower than the error. The low estimated standard deviations are explained by the simple models chosen for dynamics and sensors in this paper. Unmodeled characteristics e.g. the time varying bias of the gyroscope $\delta_\omega^S$, which is assumed to be constant in this paper or time delays in obtaining the GNSS sensor measurements influence the estimated uncertainty significantly and lead for both estimators to an overconfident estimate.

## 5. CONCLUSION & FUTURE WORK

We proposed an estimation framework for sensor fusion of GNSS amd IMU based on methods from direct optimal

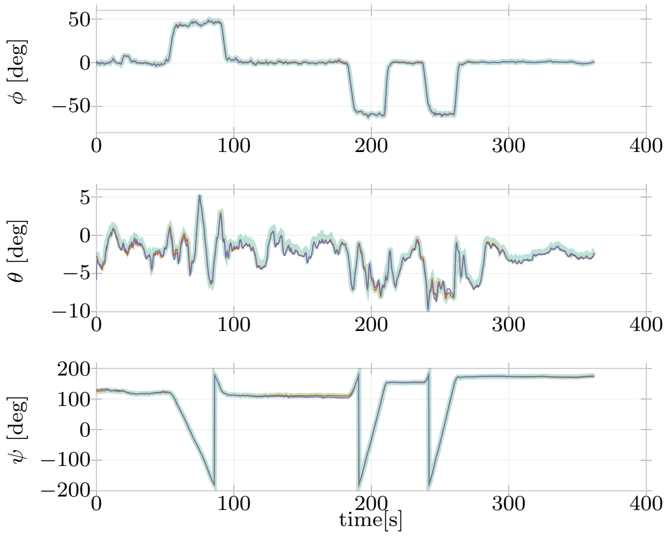


Fig. 5. Estimation results of orientation for batch (—) and filter (—) in Euler angles roll $\phi$, pitch $\theta$ and yaw $\psi$ compared to the reference (—) trajectory.

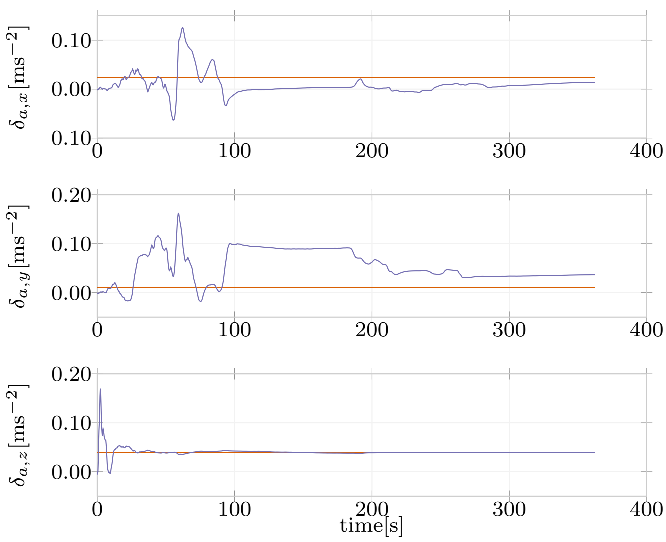


Fig. 6. Estimation results of accelerometer bias for batch (—) and filter (—) estimator.

control with a versatile structure that allows a batch and filter implementation. The developed estimators were evaluated against an accurate reference for a strongly maneuvering aircraft and yield low RMSEs. The filter approach suffers from limited observability resulting in erratic identification of sensor parameters and causing drifting state estimates.

We plan to improve the accuracy and robustness of the approach by extending the set of estimated sensor parameters to include scale factors of the IMU and considering more detailed dynamic models. This will allow for the inference of aerodynamic parameters and a complete in-run sensor calibration. Further work will also focus on improving the computational efficiency of the approach to yield a real-time compliant implementation for embedded systems. To allow for such without compromising on the robustness of the batch estimator, we are considering to extend the proposed framework to include *moving horizon estimation*

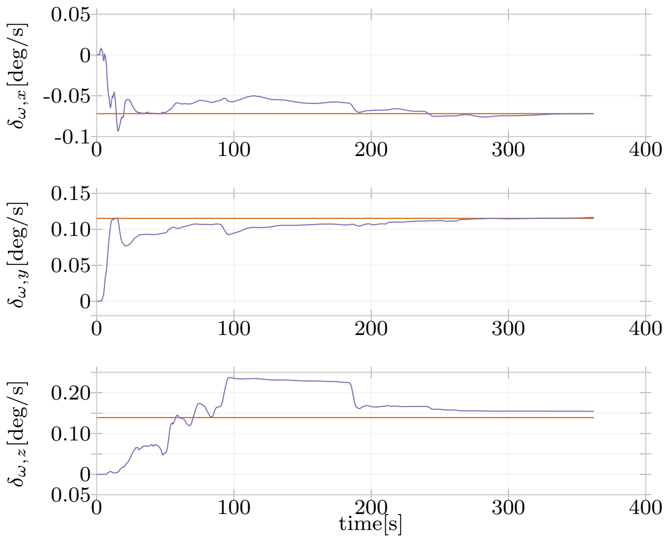


Fig. 7. Estimation results of gyroscope bias for batch (—) and filter (—) estimator.

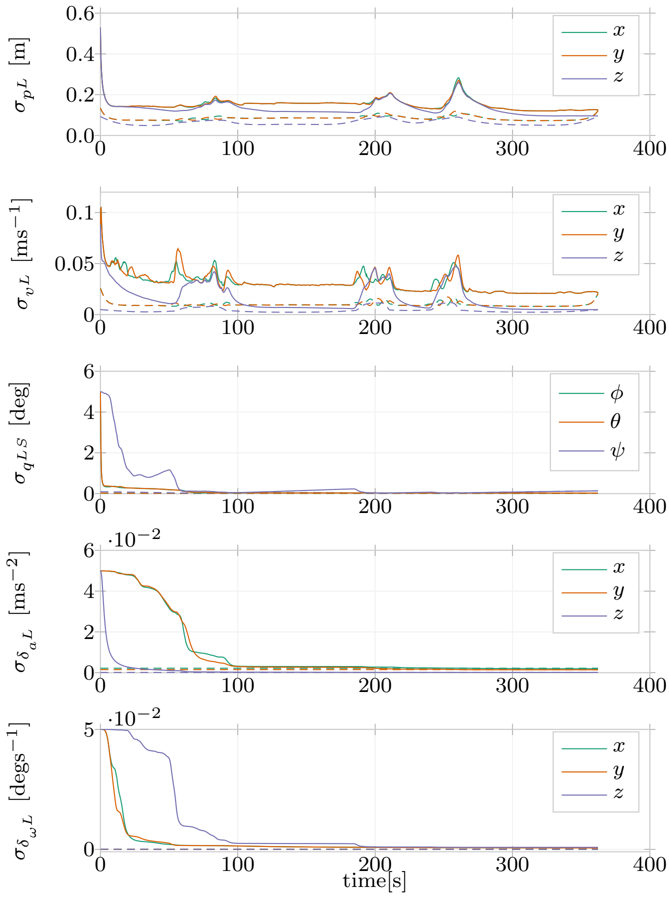


Fig. 8. Estimated standard deviations of position, velocity, orientation and biases for batch (–) and filter (--) over estimation horizon.

(MHE) as promising further step towards robust sensor fusion.

## REFERENCES


Ahrens, U., Diehl, M., and Schmehl, R. (eds.) (2013). *Airborne Wind Energy*. Green Energy and Technology. Springer Berlin Heidelberg, Berlin, Heidelberg. doi: 10.1007/978-3-642-39965-7.

Andersson, J. (2013). *A General-Purpose Software Framework for Dynamic Optimization*. Phd thesis, Arenberg Doctoral School, KU Leuven, Heverlee, Belgium.

Grabe, V., Bülthoff, H.H., Scaramuzza, D., and Giordano, P.R. (2015). Nonlinear ego-motion estimation from optical flow for online control of a quadrotor UAV. *The International Journal of Robotics Research*, 34(8), 1114–1135. doi:10.1177/0278364915578646.

Grewal, M.S., Weill, L.R., and Andrews, A.P. (2007). *Global positioning systems, inertial navigation, and integration*. John Wiley & Sons.

Gros, S., Zanon, M., and Diehl, M. (2012). Orbit control for a power generating airfoil based on nonlinear MPC. doi:10.1109/ACC.2012.6315367.

Hol, J.D., Dijkstra, F., Luinge, H., and Schon, T.B. (2009). Tightly coupled UWB/IMU pose estimation. In *2009 IEEE International Conference on Ultra-Wideband*, 688–692. IEEE. doi:10.1109/ICUWB.2009.5288724.

Iwata, K. (2013). Research of Cargo UAV for civil transportation. *Journal of Unmanned System Technology*, 1(3), 89–93. doi:10.21535/JUST.V1I3.40.

Kameswaran, S. and Biegler, L.T. (2008). Convergence rates for direct transcription of optimal control problems using collocation at Radau points. *Computational Optimization and Applications*, 41(1), 81–126. doi: 10.1007/s10589-007-9098-9.

Laks, J.H., Pao, L.Y., and Wright, A.D. (2009). Control of wind turbines: Past, present, and future. In *2009 American Control Conference*, 2096–2103. IEEE. doi: 10.1109/ACC.2009.5160590.

Perez, D., Maza, I., Caballero, F., Scarlatti, D., Casado, E., and Ollero, A. (2013). A Ground Control Station for a Multi-UAV Surveillance System. *Journal of Intelligent & Robotic Systems*, 69(1-4), 119–130. doi: 10.1007/s10846-012-9759-5.

Polóni, T., Rohal-Ilkiv, B., and Arne Johansen, T. (2015). Moving Horizon Estimation for Integrated Navigation Filtering. *IFAC-PapersOnLine*, 48(23), 519–526. doi: 10.1016/j.ifacol.2015.11.331.

Savage, P.G. (1998). Strapdown Inertial Navigation Integration Algorithm Design Part 1: Attitude Algorithms. *Journal of Guidance, Control, and Dynamics*, 21(1), 19–28. doi:10.2514/2.4228.

Titterton, D. and Weston, J.L. (2004). *Strapdown inertial navigation technology*. Institution of Electrical Engineers. doi:10.1049/PBRA017E.

Vandersteen, J., Diehl, M., Aerts, C., and Swevers, J. (2013). Spacecraft Attitude Estimation and Sensor Calibration Using Moving Horizon Estimation. *Journal of Guidance, Control, and Dynamics*, 36(3), 734–742. doi:10.2514/1.58805.

Vydhyanathan, A., Bellusci, G., Luinge, H., and Slycke, P. (2015). The Next Generation Xsens Motion Trackers for Industrial Applications. URL `https://www.xsens.com`.

Wächter, A. and Biegler, L.T. (2006). On the implementation of an interior-point filter line-search algorithm for large-scale nonlinear programming. *Mathematical Programming*, 106(1), 25–57. doi:10.1007/s10107-004-0559-y.